ACS APPLIED MATERIALS & INTERFACES

Research Article

www.acsami.org

Monolithically Integrated Micro- and Nanostructured Glass Surface with Antiglare, Antireflection, and Superhydrophobic Properties

Domenico Tulli,[†,‡] Shandon D. Hart,[§] Prantik Mazumder,[§] Albert Carrilero,[†] Lili Tian,[§] Karl W. Koch,[§] Ruchirej Yongsunthon,[§] Garrett A. Piech,[§] and Valerio Pruneri*[,†,⊥]

[§]Corning Incorporated, Sullivan Park, Corning, New York 14831, United States

[†]Institut de Ciències Fotòniques, Avenida Carl Friedrich Gauss 3, 08860 Castelldefels, Barcelona, Spain

[⊥]Institució Catalana de Recerca i Estudis Avançats, Passeig Lluís Companys 23, 08010 Barcelona, Spain

ABSTRACT: Hierarchical micro- and nanostructured surfaces have previously been made using a variety of materials and methods, including particle deposition, polymer molding, and the like. These surfaces have attracted a wide variety of interest for applications including reduced specular reflection and superhydrophobic surfaces. To the best of our knowledge, this paper reports the first monolithic, hierarchically structured glass surface that combines micro- and nanoscale surface features to simultaneously generate antiglare (AG), antireflection (AR), and superhydrophobic properties. The AG microstructure mechanically protects the AR nanostructure during wiping and smudging, while the uniform composition of the substrate and the micro- and nanostructured surface enables ion exchange through the surface, so that both the substrate and structured surface can be simultaneously chemically strengthened.

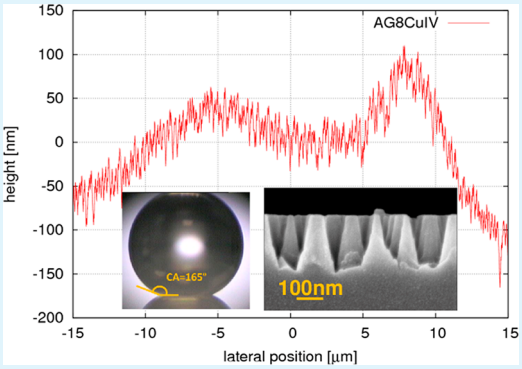

KEYWORDS: *antiglare, antireflection, superhydrophobicity, monolithic, hierarchical, micro/nanostructuring*

INTRODUCTION

The typical surface reflectivity (about 4% under normal incidence) of glass or polymers reduces the performance, and in some cases the lifetime, of displays and other optical devices: for example, spurious reflection of sunlight or bright objects can corrupt the user's view of an image from a display or optical loss and instability of a laser cavity can be caused by back-reflection. In recent years, much effort has been put into design optimization of the front surfaces of optics and information displays. More specifically, antireflection (AR) and/or antiglare (AG) surfaces have been developed to improve image contrast and clarity in displays. First, conventional AR coatings with single-layer or multilayer thin films were employed to reduce the reflection.[1,2] These coatings are based on the destructive interference of multiple reflections from the surface structure. While the performance could be high, the approach suffers from several drawbacks, including narrow wavelength response and/or angular sensitivity, sensitivity to film thickness variation, thermal expansion mismatch, reduced substrate adhesion on certain materials, and susceptibility to scratching. Lately, biomimetic subwavelength structures inspired by the Moth-eye[3−9] have attracted great interest because of their high performance and potential low cost.[10−13] The AR effect comes from a smooth refractive index gradient at the interface, associated, for example, with nanopillars comprising a conical shape. When the nanopillars have a subwavelength dimension, light scattering becomes negligible, thus preserving the directionality of the transmitted beams and the clarity of the surface.

Another way to suppress reflection effects is to use an AG surface treatment. AG surfaces use diffusion mechanisms to scatter the light that is reflected from a surface or an interface.[14] Diffusion reduces the specularity of the reflected image from the external environment, making unwanted images unfocused to the eye and thereby reducing eyestrain or distraction when the intended image contained in the display is viewed. However, the suppression of unwanted reflections can simultaneously sacrifice the clarity, contrast, and resolution of the transmitted image, and often displays using AG surfaces do not achieve a satisfactory performance. An AG surface can be obtained through appropriate texturing of the surface.[15] Various techniques have been developed including grinding, holographic exposure techniques, etching with an acidic solution, and self-assembled nanoparticle coatings.[16−19] To improve the clarity and contrast of an AG surface, especially in intense ambient light conditions, AR nanostructures have been effectively applied on top of AG surfaces. In this case, AG and AR structures have mainly been produced by injection molding and hot-embossing, for example, in polymeric films.[11,19,20]

Received: March 4, 2014
Accepted: June 24, 2014
Published: June 24, 2014

On the other hand, hierarchical micro- and nanostructured surfaces having combined AG and AR properties have never been formed in a monolithic, uniform composition glass surface. While glass has desirable characteristics for many applications (scratch resistance, UV and temperature tolerance, laser damage tolerance, etc.), it is difficult to apply the above-mentioned polymer-molding techniques to glass because the relatively high viscosity of glass at practical molding temperatures prevents high-fidelity molding of nanostructures. Raising the glass temperature to a point where it is less viscous will tend to damage any practical master mold material, as well as render any practical substrate nonflat or otherwise distorted. In this paper, we describe a novel glass surface with combined AR and AG properties. The AG and AR properties are obtained by micro- and nanostructures directly fabricated on the glass surface. In addition to the coveted optical properties, superhydrophobic (or superhydrophilic) self-cleaning characteristics are also achieved on the glass surface, rendering the latter superhydrophobic (or superhydrophilic), AG, AR, transparent substrate. The proposed method consists of first creating an AG surface (lateral length scale ~1−100 μm; vertical length scale ~10−500 nm) followed by creating nanotextures (lateral length scale ~10−300 nm; vertical length scale 10−300 nm) superposed on the AG surface. AR nanostructures are fabricated on AG microstructures by reactive ion etching (RIE) through a nanomask, which is formed by dewetting ultrathin (<10 nm) copper films subjected to rapid thermal annealing (RTA). This leads to a two-tier hierarchical surface geometry that offers excellent AG and AR properties together. The AG microstructure seems to protect the AR nanostructure thanks to its larger protrusions, as shown by wiping experiments. By taking advantage of the designed composition of the glass, one could ion exchange the substrate and micro- and nanostructured surface simultaneously and thereby provide additional mechanical strength, a highly desirable feature for many applications, such as displays or touchscreens. As expected, we show that AR combined with AG gives an improved visual appearance (less visible specular reflections) compared to AR alone. In addition, it also provides extremely high superhydrophobicity compared to a AG or AR surface alone.

RESULTS AND DISCUSSION

Fabrication of AG and AR Structures. One way to achieve AG and reduce the intensity of the specular reflection is to roughen the glass surface or cover it with a textured film. The dimension of the roughness should be large enough to scatter visible light, resulting in a hazy or matte surface, but not so large so as to diminish the transparency of the glass. AG surfaces were produced by applying a particulate polymer mask to the glass surface, fusing the particles to the glass surface, and etching the glass through the spaces in the particulate mask using a hydrofluoric/sulfuric acid mixture. Similar methods for creating AG surfaces are described in detail in ref 21. The lateral dimension of the AG textures is in the range of 1−100 μm, while the vertical length scale is typically on the order of tens to hundreds of nanometers. The AG surface was covered by copper ultrathin metal films (UTMFs) of 4 or 8 nm thickness using sputtering techniques. The continuous metal film following the AG surface morphology was subsequently dewetted at 750 °C for 95 s.[10] Figure 1 shows the process steps for the fabrication of nanopillars on AG glass substrates and summarizes the most significant parameters of the dewetted nanopillars.

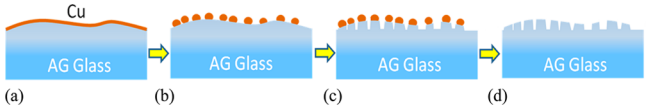

Figure 1. Creation of surface nanostructures monolithically integrated in the AG substrate. Cu UTMF is deposited on AG substrates (a). Metal dewetting is used to create metal nanoparticles from a continuous UTMF (b) and subsequent etching, for example, RIE, to produce the nanopillars on the substrate surface (c). Finally, the metal mask is removed (d).

The optical transmission measured before and after the metal dewetting process is shown in Figure 2. The formation of a well-defined dip in the optical transmission spectrum is related to local surface plasmon resonance effects of formed copper islands (i.e., nanoparticles), thus confirming that the initial continuous film has been dewetted. The dewetted metal nanoparticles are randomly distributed on top of the AG structure but are statistically uniform over the entire AG surface for large scales compared to the average pillar diameter. This uniform coverage of metal nanoparticles is important to achieving the desired combined AG and AR effects, and it is the result of our selected AG roughness profile, glass surface cleaning methods, metal deposition methods, metal film thickness, and dewetting process steps.

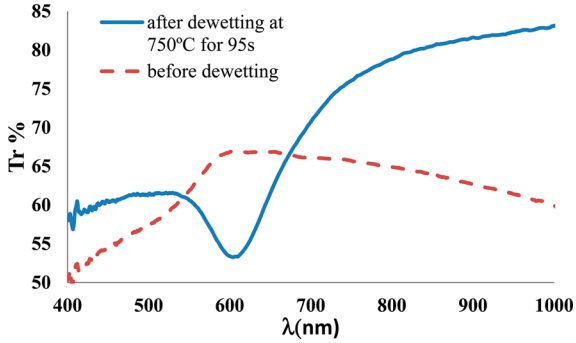

Figure 2. Optical transmission of an AG surface covered with an ultrahin copper layer (sample AG 8 Cu III), 8 nm thick, before and after dewetting. The plasmon resonance behavior is indicative of metal nanoparticle formation due to treatment at high temperature.

Localized scanning electron microscopy (SEM) images of metal nanoparticles on AG surfaces can be seen in Figure 3, which confirms uniform distribution of the dewetted metal islands. Through control of the process variables, it is possible to tailor the nanostructures as well as the optical properties. It can be noted that thicker initial films lead to lower density and larger dewetted particles (provide the thickness values and, if available, the average/root-mean-square island diameters showing the effect of the initial thickness on the island diameter). Subsequently, samples were RIE-etched to create nanopillars. The details of the process can be found in a previously published paper.[10]

In Figure 4 (left), we show an atomic force microsopy (AFM) height image of the top surface after the etching step and after the metal nanoparticles have been removed. Figure 4 (right) shows a horizontal cross-sectional profile of the AFM height image of Figure 4 (left) at the center of the image.

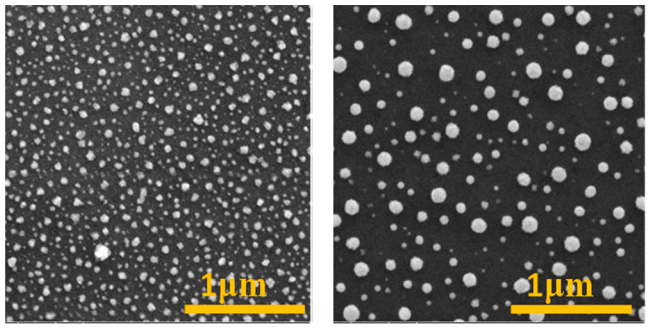

Figure 3. SEM images of the self-assembled dewetted copper nanoparticles for different copper thickness on AG surfaces: sample AG 4 Cu I (left); sample AG 8 Cu II (right).

The short-range fluctuations of the cross section indicate the etched pillars, which are in this case roughly 50 nm high. This is lower than the actual nanopillar height because of the fact that the scan pixel size is too large to accurately resolve the structure. The resulting AR glass nanopillars are better resolved in Figure 5, where the height is on the order of 200 nm.

Optical Characterization. The optical transmission and haze measured by a hazemeter (BYK-Gardner GmbH with 0°/diffuse geometry) are summarized in Table 2. The hazemeter is a single-port system with an integrating sphere and has no wavelength spectrometer capability. The port diameter size is ∼1 in., and the sphere diameter is ∼150 mm. This system tends to report a slightly higher transmission than the true value because of the single-port geometry, but the relative trend of the measurement is accurate. From Tables 1 and 2, it can be seen that the haze tends to increase with the etching time. However, the plasma etching process can also reduce the haze of the initial AG surface. This has been observed in AG surfaces with larger initial haze (about 3%) that presented haze smaller than 2.5% after etching of the conformal nanopillar structure.

The samples were then optically characterized by measuring the total, axial (specular), and diffuse transmission and reflection using a Lambda 950 UV/vis/IR system, which is periodically calibrated according to ASTM recommended procedures using absolute physical standards or standards traceable to the National Institute of Standards and Technology. In Figure 6, we show the results for four of the processed samples. One can clearly see that a flat AR effect can be obtained with high transmission and a haze level similar to or even smaller than that of the initial AG surface. With the purpose of quantifying angular scattering of the samples, angular reflected power was measured on a custom setup using collimated light from a 530 nm light-emitting diode that strikes the sample and is then focused by a f = 100 mm lens onto a CCD camera. This setup measures the angular scattering at high resolution (0.05°) but is limited to a small angular range (±2.5°) around the Fresnel reflection angle. Reflectance measurements were performed with samples mounted directly to face of the integrating sphere's exit port hole. Total reflectance was measured with the sample mounted at 8° incidence to the light beam, whereas diffuse reflectance was measured with the sample orthogonal to the light beam with the sphere's input port open. All measurements were performed with samples mounted with the treated surface toward the incident beam.

When these results were compared to the measurements of a flat glass surface, the amount of reflection haze could be calculated. Distinctness of reflected image (DOI) figures were also provided, quantifying the spread of light reflected at the specular angle:[22]

$$\mathrm{DOI} = 100 \times \frac{R_s - R_{0.3^\circ}}{R_s} \quad (1)$$

where $R_{0.3^\circ}$ is the integrated reflected power within 0.3° of the specular direction and R_s is the specular reflected power. The angular scattering of some of the samples was examined, as shown in Figure 7.

According to this figure, the light reflected is concentrated in the specular direction. These plots prove that the level of haze (which corresponds to scattering outside ±2.5° and can create a washed out or milky appearance in display applications) on the nanostructured samples is very low. The visual appearance of the AG and AG + AR (AG 8 Cu IV) samples on a black background is shown in Figure 8. One can appreciate that the AR nanostructuring increases the transparency and clarity of the sample, showing a less milky aspect as well as making the background clearer. Because of the large difference in the length

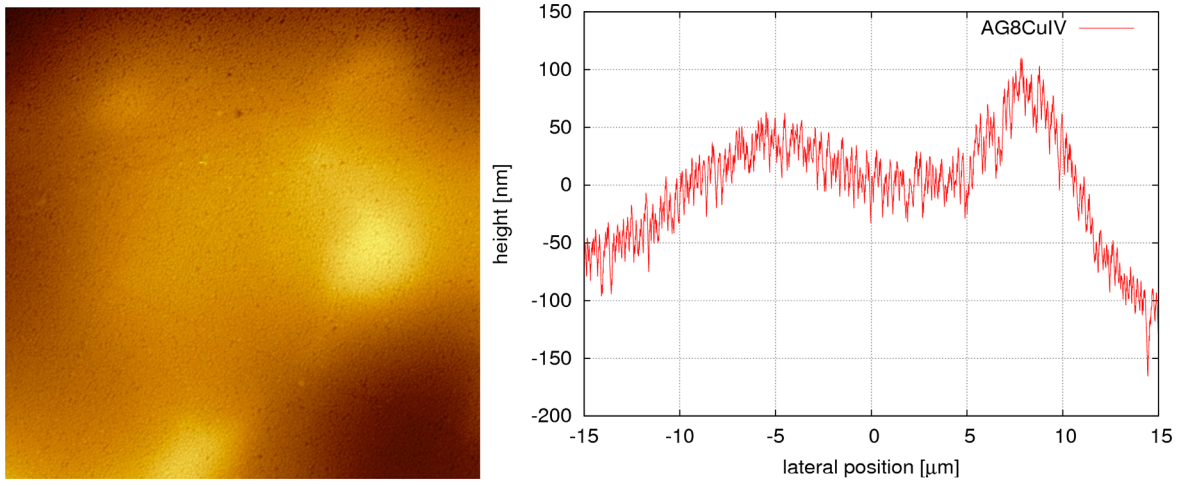

Figure 4. (left) AFM height image taken over a 30 μm × 30 μm area with a pixel size of ∼10 nm for an AG surface. The large-scale lateral features are characteristic of the AG substrate, while the fine-scale texture is the AR feature. (right) AFM scan of the height profile along a horizontal line through the center of the image. The fine-scale texture shows a vertical range of approximately 50 nm over a lateral range of ∼100 nm.

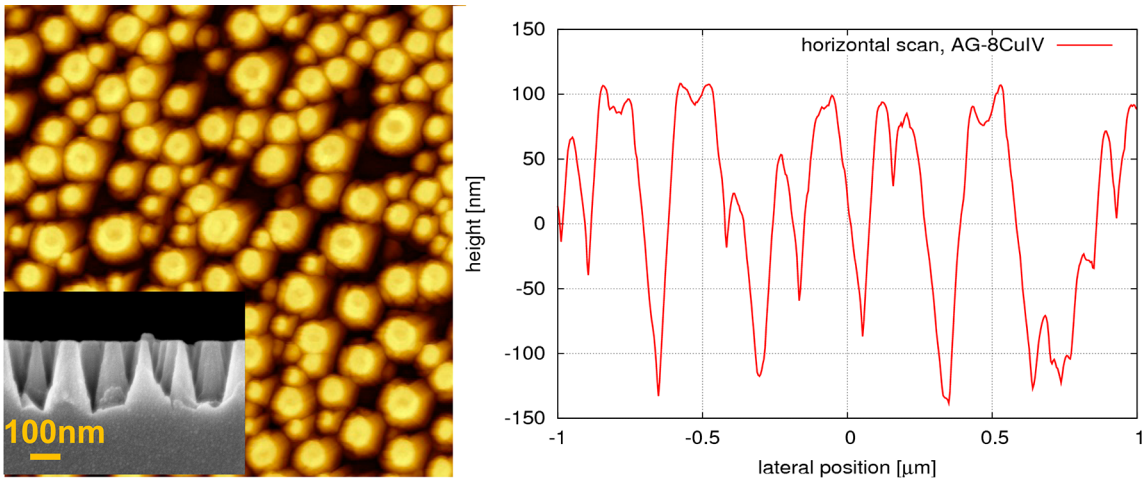

Figure 5. AFM height images and scan of the AG surfaces with the nanopillars obtained using RIE of the surface covered by dewetted metal nanoparticles: sample AG 8 Cu IV. The inset of the left figure is a SEM image of the cross section of the surface.

Table 1. Summary of the Most Significant Parameters of the Dewetted Ultrathin Copper on AG Substrates

sample ID	initial metal thickness (nm)	dewetting	dry etching time (min)
AG 4 Cu I	4	750 °C, 95 s	5
AG 4 Cu II	4	750 °C, 95 s	7
AG 4 Cu III	4	750 °C, 95 s	9
AG 8 Cu I	8	750 °C, 95 s	4
AG 8 Cu II	8	750 °C, 95 s	6
AG 8 Cu III	8	750 °C, 95 s	8
AG 8 Cu IV	8	750 °C, 95 s	10

Table 2. Optical Transmission and Haze for the Samples Processed[a]

	T (%)	haze (%)
bare AG surface	92.1	0.92
AG 4 Cu I	94.15	0.95
AG 4 Cu II	93.57	0.92
AG 4 Cu III	93.96	0.93
AG 8 Cu I	93.37	0.68
AG 8 Cu II	94.35	0.84
AG 8 Cu III	94.25	1.01
AG 8 Cu IV	93.96	1.86

[a]Values were obtained using a BYK Gardner Haze-Gard Plus hazemeter.

scales for the AR and AG textures, the physics of the two effects are essentially separable. The lateral length scale of the AG texture ranges from 10 to 100 μm, while the lateral length scale of the AR texture is on the order of 100 nm. Over length scales of the optical wavelength, the AG texture is essentially flat, although the slope of the surface may be as large as ±2°. The AR texture is still small compared to the optical wavelength and still provides AR performance, even at the small angles of the AG-textured surface.

Wetting Properties. Once the structures have been fabricated on the substrates by dry etching and the remaining metal nanoparticles have been removed, the contact angles for water were measured. The water contact angles of about 25° were similar to those of similar AR nanostructures on flat surfaces.[10] Nonetheless, their performance can be fully transformed by activating the sample surfaces with the fluorosilane coating Dow Corning 2634 using a simple process.[23] A contact angle as high as ≥165° in some samples was achieved (Figure 9, left), a value significantly higher than that of the only AR surface made with nanopillars (140–150°).[10] This indicates that the underlying AG roughness significantly contributes to the superhydrophobic behavior. This is likely due to the fact that the high roughness of the AG surface leads to larger freely suspended water meniscus in air than would have been achieved by the AR structure alone. In the absence of any underlying AG structure, the water droplet is perched on top of the nanopillars in the Cassie–Baxter state. In this configuration state, almost all, if not all, of the nanopillars' top surfaces are wetted by the water droplet and the fraction of wetted area is approximately given by the fraction of the nanopillar top surface area. In the presence of a large undulation underneath the nanopillars, it is likely that some of the nanopillar top surfaces are not wetted by the water because the meniscus of the latter is suspended above them. Also, the contact angle hysteresis on this surface was very low, leading to easy roll off of the droplet. These features should enable self-cleaning properties of the surface.

Mechanical Robustness. In order to analyze the structures' mechanical durability, a wipe test was performed using a fiber cloth with an AATCC crockmeter (SDLAtlas CM-5) and a force of 6 N over a surface of 2 cm^2. The crockmeter test consisting of 10 and 100 wipes was performed on the sample AG 8 Cu II (Figure 9, right), and the resultant optical transmission and water contact angles were measured. The optical transmission was initially reduced by about 0.5% after 10 wipes and then remained fairly constant after 100 wipes. The contact angle for water decreased only slightly, ∼4% after 100 wipes (from 165° to 158°). The corresponding rolling-off angle was below 10°. This shows that the more pronounced AG microstructure protects the AR nanostructure without the need of any additional treatment. In fact, in a previous publication,[10] it was demonstrated that ion exchange can further increase the mechanical resistance of the nanostructures and hence of the whole surface. During the process involving an alkali-containing glass, Na ions in the substrate are replaced by larger K ions, thus creating a layer of compressive stress throughout the nanostructured glass surface.[24] By using ion exchange, one can thus increase further the mechanical resistance of the AR nanostructures if need be.

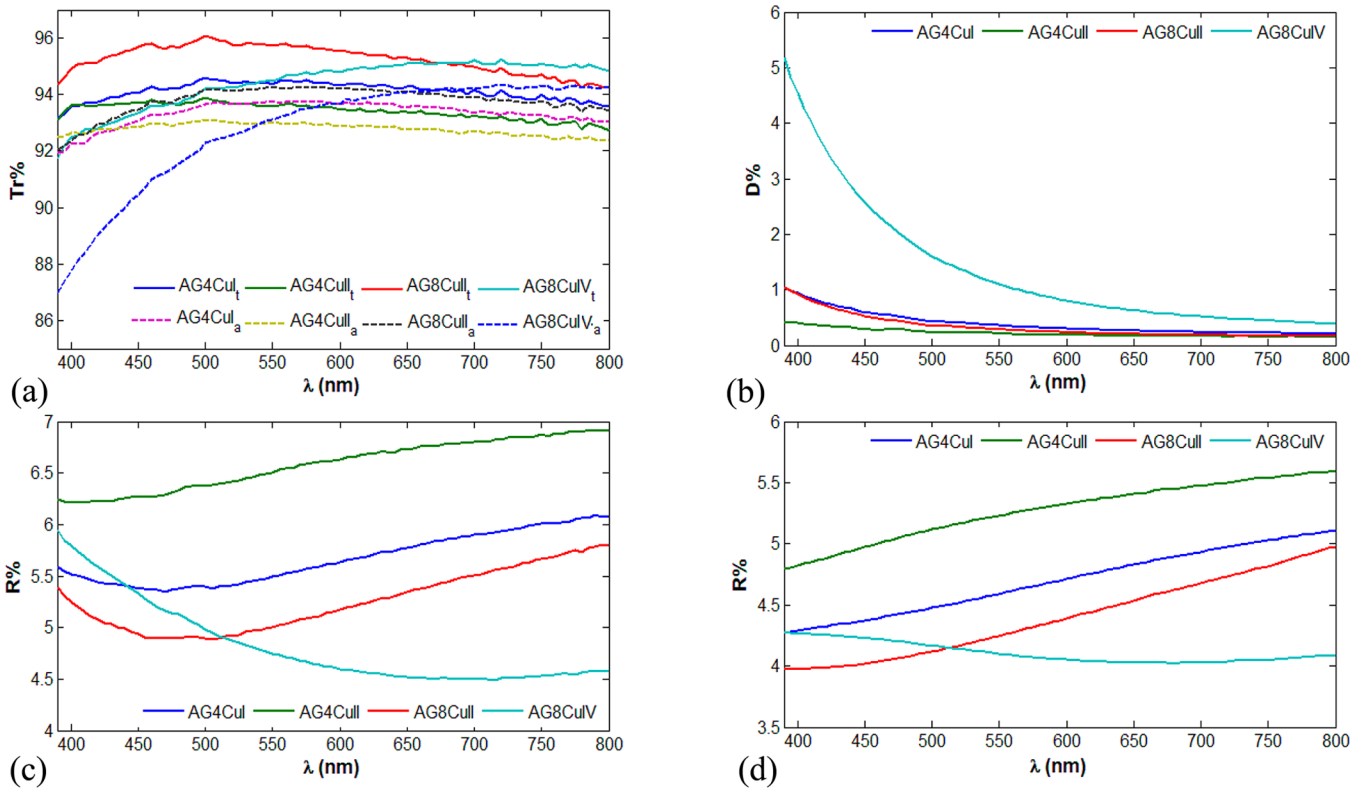

Figure 6. Total and axial (direct) (a) and diffuse (b) optical transmission from a substrate of AG + AR structures. Total (c) and specular (d) reflectivity as a function of the wavelength for a series of different dewetting processes: AG 4 Cu I and II and AG 8 Cu II and IV. Note that only one side of the glass is treated with the AG + AR structure, and the non-AR side of the glass is expected to reflect about 4%, which represents the minimum % *R* achievable for a one-side AR-treated glass. The total reflectance for a glass with AG alone (and no AR) is expected to be about 8%.

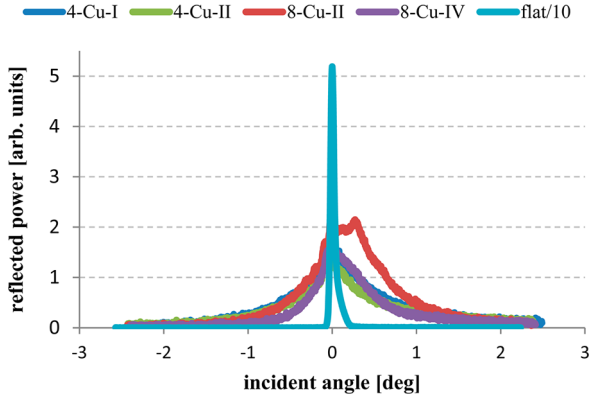

Figure 7. Angular reflected power plot for different micro- and nanostructured AG and AR samples. The narrower curve, obtained from the flat glass, has been scaled down by a factor of 10 for comparison.

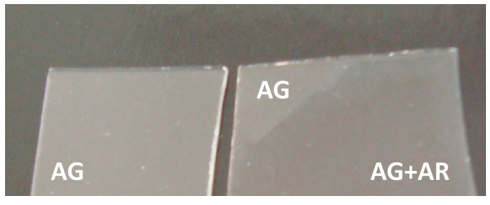

Figure 8. Photographs of micro- and nanostructured AG (left) and AG + AR (right) samples. The AG + AR sample is sample AG 8 Cu IV and has a corner without the AR nanostructure, highlighting the difference between AG and AG + AR.

CONCLUSIONS

Optimal viewing comfort and display ergonomics can be achieved by a combination of AR and AG properties. We have investigated a novel textured glass substrate that combines micro- and nanoscale features to confer both properties at the same time. To the best of our knowledge, this is the first time that hierarchical micro- and nanostructures having AG and AR properties are combined on a glass surface in a monolithic manner. The chosen structures are fabricated by dry etching of a thermally dewetted copper nanomask, conformally created on an AG surface by polymer masking and wet etching. The geometry of the nanoparticles forming the nanomask can be changed by selecting the initial metal thickness and RTA process parameters. The average reflectance of the treated samples is in this way reduced, while transmission is increased and haze remains unchanged relative to the AG surface. The surface is hydrophilic and can become superhydrophobic by applying a fluorosilane coating. With respect to fluorosilane-coated glass, there is a strong increase in the water contact angle due to both the AR nanostructures and AG microstructures. The presence of the AG structures and the possibility of ion exchange of the glass substrates allow enhancement of the mechanical durability and robustness. The proposed method relies on inexpensive lithography-free fabrication techniques and can be industrialized to produce large AG and AR glass surfaces with broad-band low reflectivity, low haze, high transmission, and mechanical durability.

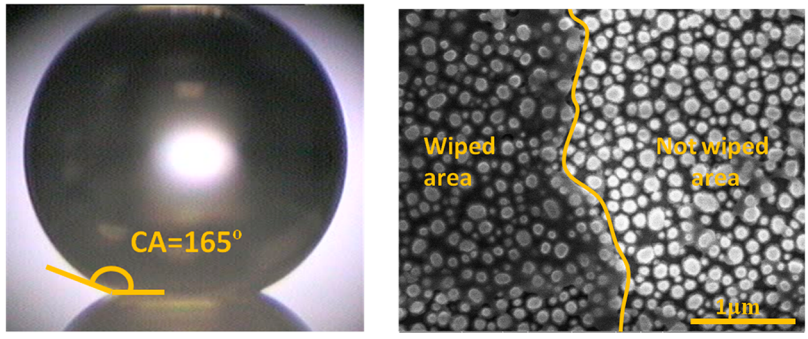

Figure 9. (left) 2 mL water droplet on the superhydrophobic AG + AR surface coated with fluorosilane. (right) SEM image of the sample AG 8 Cu II, not ion exchanged, after crockmeter tests with 100 wipes with a fiber cloth applying a force of 6 N over a surface of 2 cm^2. Note that the initial water contact angle decreased about 3% after 10 wipes and an additional 3% after 100 wipes. Protection of the nanostructuring due to AG roughness can be further increased by ion exchange.[10]

AUTHOR INFORMATION

Corresponding Author

*E-mail: valerio.pruneri@icfo.es.

Present Address

‡Department of Electrical and Computer Engineering, University of California, Davis, CA 95616.

Author Contributions

The manuscript was written through contributions of all authors. All authors have given approval to the final version of the manuscript.

Notes

The authors declare no competing financial interest.

REFERENCES

(1) MacLeod, H. A. *Thin Film Optical Filters*; Elsevier: New York, 1968.

(2) Lowdermilk, W. H.; Milam, D. Graded-Index Antireflection Surfaces for High-Power Laser Applications. *Appl. Phys. Lett.* **1980**, *36*, 891−893.

(3) Parker, A. R.; Townley, H. E. Biomimetics of Photonic Nanostructures. *Nat. Nanotechnol.* **2007**, *2*, 347−353.

(4) Chen, J. Y.; Chang, W. L.; Huang, C. K.; Sun, K. W. Biomimetic Nanostructured Antireflection Coating and its Application on Crystalline Silicon Solar Cells. *Opt. Express* **2011**, *19*, 14411−14419.

(5) Gombert, A.; Glaubitt, W.; Rose, K.; Dreibholz, J.; Bläsi, B.; Heinzel, A.; Sporn, D.; Döll, W.; Wittwer, V. Subwavelength-Structured Antireflective Surfaces on Glass. *Thin Solid Films* **1999**, *351*, 73−78.

(6) Min, W.-L.; Jiang, B.; Jiang, P. Bioinspired Self-Cleaning Antireflection Coatings. *Adv. Mater.* **2008**, *20*, 3914−3918.

(7) Li, Y.; Zhang, J.; Zhu, S.; Dong, H.; Jia, F.; Wang, Z.; Sun, Z.; Zhang, L.; Li, Y.; Li, H.; Xu, W.; Yang, B. Biomimetic Surfaces for High-Performance Optics. *Adv. Mater.* **2009**, *21*, 4731−4734.

(8) Zhu, J.; Hsu, C.-M.; Yu, Z.; Fan, S.; Cui, Y. Nanodome Solar Cells with Efficient Light Management and Self-Cleaning. *Nano Lett.* **2009**, *10*, 1979−1984.

(9) Bernhard, C. G. *Structural and Functional Adaptation in a Visual System*; Endeavour Press: London, 1967; Vol. *26*.

(10) Infante, D.; Koch, K.; Mazumder, P.; Tian, L.; Carrilero, A.; Tulli, D.; Baker, D.; Pruneri, V. Durable, Superhydrophobic, Antireflection, and Low Haze Glass Surfaces Using Scalable Metal Dewetting Nanostructuring. *Nano Res.* **2013**, *6*, 429−440.

(11) Taguchi, T.; Hayashi, H.; Fujii, A.; Tsuda, K.; Yamada, N.; Minoura, K.; Isurugi, A.; Ihara, I.; Itoh, Y. Ultra-Low-Reflective 60-in. LCD with Uniform Moth-Eye Surface for Digital Signage. *Dig. Technol. Pap., Soc. Inf. Dispersion Int. Symp.* **2010**, *41*, 1196−1199.

(12) Hobbs, D. S.; MacLeod, B. D.; Riccobono, J. R. In *Update on the Development of High Performance Anti-Reflecting Surface Relief Micro-Structures*; Window and Dome Technologies and Materials X Proceedings; SPIE: Bellingham, WA, 2007; p 65450Y.

(13) Wilson, S. J.; Hutley, M. C. The Optical Properties of 'Moth Eye' Antireflection Surfaces. *Opt. Acta* **1982**, *29*, 993−1009.

(14) Nuijs, A. M.; Horikx, J. J. L. Diffraction and Scattering at Antiglare Structures for Display Devices. *Appl. Opt.* **1994**, *33*, 4058−4068.

(15) Kelley, E. Sensitivity of Display Reflection Measurements to Apparatus Geometry. *Dig. Technol. Pap., Soc. Inf. Dispersion Int. Symp.* **2002**, *33*, 140−143.

(16) Kawamura, T.; Kawamura, H.; Kobara, K.; Endo, Y. Image Display Panel Having Antistatic Film with Transparent and Electro-conductive Properties and Process for Processing Same. U.S. Patent 4,945,282, July 31, 1990.

(17) 3M Graphic Solution. http://solution.3m.com (accessed Apr 2, 2013).

(18) Durauve Protection. www.tspinc.com (accessed Nov 7, 2013).

(19) Boerner, V.; Abbott, S.; Bläsi, B.; Gombert, A.; Hoßfeld, W. Holographic Antiglare and Antireflection Films for Flat Panel Displays. *Dig. Technol. Pap., Soc. Inf. Dispersion Int. Symp.* **2003**, *34*, 68−71.

(20) Gombert, A.; Lerchenmüller, H. Antireflection Coating and Method of Manufacturing the Same. U.S. Patent 6,359,735, Mar 19, 2002.

(21) Gollier, J.; Hart, S. D.; Nguyen, K.; Alan, T. S. I. I.; West, J. A.; Zhang, L. Glass Having Antiglare Surface with Low Display Sparkle. U.S. Patent 2012/0218640, Aug 30, 2012.

(22) Hunterlab. Insight on Color, Applications Note: Distinctness of Reflected Image (DOI), http://www.hunterlab.com/appnotes/an09_97.pdf (accessed Nov 13, 2013).

(23) Dow Corning 2634 coating, http:www2.dowcorning.com/datafiles/090007c880276ab9.pdf (accessed Apr 2, 2013).

(24) Mochel, E. L. Mechanical Strengthening of Glass by Ion Exchange. U.S. Patent 3,485,702, Dec 23, 1969.